Effect of Ti-doping on the Electrochemical Performance of Lithium Vanadium(III) Phosphate

S. M. Stankov[1*], I. Abrahams[2**], A. Momchilov[1], I. Popov[1], T. Stankulov[1], A. Trifonova[3]

[1] *Institute of Electrochemistry and Energy Systems "Acad. Evgeni Budevski" - Bulgarian Academy of Sciences, Acad. Georgi Bonchev Str., Block 10, 1113 Sofia, Bulgaria*

[2] *Materials Research Institute, School of Biological and Chemical Sciences, Queen Mary University of London, Mile End Road, London E1 4NS, United Kingdom*

[3] *AIT Austrian Institute of Technology GmbH, Giefinggasse 2, 1210 Vienna, Austria*

Corresponding authors:

* s.stankov@mail.bg

** i.abrahams@qmul.ac.uk

Abstract

Carbon coated and titanium substituted lithium vanadium phosphate composites have been successfully prepared through a sol-gel method followed by solid state reaction under argon. $Li_3V_{1.9}Ti_{0.1}(PO_4)_3$-C (LVT10PC) and $Li_3V_{1.85}Ti_{0.15}(PO_4)_3$-C (LVT15PC) were investigated using X-ray powder diffraction, thermal analysis, transmission electron microscopy, cyclic voltammetry and galvanostatic tests. Different models for the solid solution mechanism in this system are discussed. Electrochemical tests, at a charge-discharge rate of 0.2C, in the range 2.8-4.4 V, show that LVT10PC delivers the highest discharge capacity of 121 mA h g^{-1} and declines to 115.7 mA h g^{-1}, up to the 60th cycle, corresponding to a 4.4% loss. At low levels, titanium substitution is found to increase initial discharge capacity, compared to the carbon coated unsubstituted system (LVPC). Further substitution is found to have detrimental effects on initial discharge capacity and cycling behaviour.

Keywords: Lithium vanadium phosphate, positive active material, Li-ion battery, electrochemical performance.

1. Introduction

The storage of electrical energy is a key element in the development of future technologies particularly in areas such as transport and alternative energy production (solar and wind). Among battery systems, lithium-ion systems are arguably the most advanced, but the technology is currently too expensive, for widespread large-scale application. In particular, alternatives to the current generation of cathode materials, such as the expensive and toxic $LiCoO_2$ [1], are being sought to meet the requirements of high energy density and long cycle-life. In addition, systems should be environmental benign and inexpensive. One of the materials which meets these requirements and has been implemented in the industry is $LiFePO_4$ [2]. Other phosphate and flourophosphate materials such as $Li_3V_2(PO_4)_3$ [3,4], $LiMnPO_4$ [5], $LiCoPO_4$ [6], $LiNiPO_4$ [7], $LiVPO_4F$ [8] *etc*. are considered to be the next generation of commercial cathodes due to their higher output voltage and energy density compared to $LiFePO_4$. However, these materials have some drawbacks that hinder their commercialization, such as low electronic and ionic conductivity and instability during operation [9,10]. Although the problem of low electronic conductivity has been addressed for some of these materials by applying so-called carbon coating [11-13], other issues like short cycle-life remain.

The high theoretical specific capacity of lithium vanadium(III) phosphate, $Li_3V_2(PO_4)_3$ (LVP), with a value of 197 mA h g^{-1} for removal of three moles of lithium per mole, makes it of particular interest. Four characteristic plateaus are observed on de-intercalation versus Li/Li^+ at 3.6 and 3.68 V, 4.2 V and over 4.5 V, the first two of which correspond to the first lithium extraction, with the higher potentials corresponding to second and third lithium extractions [14]. Unfortunately, a decline in discharge capacity at high potentials limits the operational voltage range from 3.0 to 4.4 V [15,16] and reduces the theoretical specific capacity to ~131.5 mA h g^{-1} for two moles of lithium per mole LVP. This decline in capacity at high potentials is associated with structural instability. Partial substitution of vanadium and or phosphorus represents one possible route to greater stability. Vanadium substitution with Cr, Mo, Y, Al *etc*. [17-20] has been carried out, while anion substitution has also been investigated, for example through substitution by Cl [20]. In the present work, we investigate aliovalent substitution of V^{III} by Ti^{IV} in LVP. To our knowledge, only two previous studies have examined titanium substitution in LVP. Matesheyna and Uvarov [21] studied the di-substituted system $Li_3Mg_{0.1}Ti_{0.1}V_{1.8}(PO_4)_3$ and found no improvement in electrochemical performance in the substituted system. Liu *et al*. [22] studied the single substituted system and found that $Li_{2.8}V_{1.8}Ti_{0.2}(PO_3)_3$ exhibited an orthorhombic structure, with improved electrochemical performance. Here we examine the effect of low levels of Ti substitution on the electrochemical performance of LVP, whilst in the monoclinic phase in two representative compositions.

2. Experimental

2.1 Preparations

Carbon coated samples of $Li_3V_{2-x}Ti_x(PO_4)_3$ (x = 0.10 and 0.15) , were synthesized via a three-step sol-gel method. Stoichiometric amounts of V_2O_5 (synthesized by decomposition of NH_4VO_3 at 320°C, Fluka, >99%) and $H_2C_2O_4.2H_2O$ (Sigma-Aldrich, ≥98.5%) were dissolved in distilled water to give a blue solution (*ca*. 0.7 and 1.4 mol dm^{-3} for V^{5+} and $C_2O_4^{2-}$, respectively) To this was added separate solutions of stoichiometric amounts of $LiOH.H_2O$ (Sigma-Aldrich, ≥98%) and $(NH_4)H_2PO_4$ (Sigma-Aldrich, ≥98%) dissolved in distilled water (ca. 2.21 mol dm^{-3} for

both Li^+ and PO_4^{3-}. NH_2CH_2COOH, (glycine, Sigma-Aldrich, ≥98.5%) dissolved in distilled water (*ca*. 1.32 mol dm^{-3}) was used a carbon source and added to the above solution. The preliminary calculations were for ~6% carbon coating. To amount of glyciene added was based on tests of glyciene combustion under identical conditions to the sample. The final solution was evaporated with constant stirring at 80 °C for *ca.* 4 h until gelation occurred. Stoichiometric amounts (for x = 0.10 and 0.15) of TiO_2 powder (Sigma-Aldrich >99%) were added to the gel and thoroughly stirred until homogeneously dispersed. The mixture was dried in an oven at 120 °C for 16 h. The resulting precursor was heated at 370 °C for 4 h under flowing argon, to remove the ammonia and water. After cooling, the sample was ground for 30 min and then annealed at 800 °C for 10 h under Ar.

2.2 Sample characterisation

X-ray powder diffraction (XRD) data were collected on a PANalytical X'Pert Pro diffractometer, fitted with an X'Celerator detector, using Ni-filtered Cu-Kα radiation (λ = 1.5418 Å), over the 2θ range 5-120°, with a step width of 0.033° and an effective scan time of 200 s per step at room temperature. Diffraction data were modelled by Rietveld analysis using the GSAS suite of programmes [23]. The structure of $Li_3V_2(PO_4)_3$ [24] was used as a starting model. A small amount (*ca*. 1% by weight) of VO was included as a secondary phase, with a starting model based on the structure presented by Loehman *et al*. [25].

Thermogravimetric (TGA) and differential thermal (DTA) analyses were carried out in air on a Stanton Redcroft STA 1500 thermal analyser, in the range 20-760 °C, at a heating rate of 20°C per min. Transmission Electron Microscopy (TEM) was carried out on a JEOL JEM 2010 microscope, with an accelerating voltage of 200 kV and a beam current of 106 μA. The evaluation of specific surface area (SSA) was performed by the Brunauer-Emmett-Teller (BET) method on a Strohlein & Co. Area instrument.

2.3 Electrochemical testing

The obtained materials were tested electrochemically in two-electrode laboratory cells. The working electrodes were prepared by mixing the active material (AM), PVDF (MTI corp., USA) and acetylene black (AB) P1042 in N-methyl-2-pyrrolidone (NMP, MTI corp., USA). The ratio of the slurry was AM:PVDF 70:10 wt.% as the remaining 20 wt% consisted of acetylene black and the carbon coating of the active material. The slurries were stirred for 24 h and then coated onto aluminum foil. The coated foils were dried under vacuum at 120 °C for 24 h. Cells were assembled using lithium foil (Alfa Aeser) as the counter electrode, with Freudenberg FS 2190 as a separator. The electrolyte used was 1M $LiClO_4$ (Alfa Aeser) in a 1:1 (v/v) mixture of ethylene carbonate (EC) and dimethyl carbonate (DMC) (both purchased from Alfa Aeser). Electrochemical galvanostatic tests were performed on a Neware Battery Testing System (V-BTS8-3) in the voltage ranges 2.8 - 4.4 V, at a C/5 (0.2C) rate, where C is the theoretical specific capacity for 3 moles of extracted Li, i.e. ~197 mA h g^{-1} and 5 is the charge or discharge time in hours.

Cyclic voltammetry (CV) was performed on a VersaSTAT MC (Princeton Applied Research) multi-channel potentiostat/galvanostat, in the voltage range 2.8 - 4.8 V, with a step rate of 20 μV s^{-1}, where the counter Li electrode was also used as a reference as its polarization is negligible.

3. Results and Discussion

The fitted diffraction profiles for $Li_3V_{1.9}Ti_{0.1}(PO_4)_3$-C (LVT10PC) and $Li_3V_{1.85}Ti_{0.15}(PO_4)_3$-C (LVT15PC) are shown in Fig. 1, with the corresponding crystal and refinement data in Table 1. The data fitted well to the monoclinic structure of $Li_3V_2(PO_4)_3$ [24]. In both samples a small amount of vanadium is reduced to the +2 oxidation state to form VO (*ca*. 1 wt%). Volume is seen to increase with increasing titanium content and compares with a value of 874 $Å^3$ for the unsubstituted system prepared under similar conditions [26]. This is in contrast to the previously reported work [22], where at the x = 0.2 level of substitution, titanium substituted lithium vanadium phosphate was seen to have a smaller unit cell volume than the unsubstituted system, accompanied by a change in symmetry to orthorhombic. In order to explain this apparent discrepancy, it is important here to consider the possible methods of solid solution formation. Under the reaction conditions described above, three main possibilities exist for solid solution formation with the associated charge compensation.

1. Lithium vacancy formation:

$$V_V^x + Li_{Li}^x \rightarrow Ti_V^\bullet + V_{Li}^{'}$$

2. Vanadium reduction:

$$2V^{III}{}_V^x \rightarrow V^{II}{}_V^{'} + Ti^{IV}{}_V^\bullet$$

3. Titanium reduction:

$$V^{III}{}_V^x \rightarrow Ti^{III}{}_V$$

In the work by Liu *et al*. [22], the first mechanism was assumed in the formulation. In the present work, the amount of lithium in the sample was kept constant. Therefore, if the first mechanism was correct, then there would have been an excess of lithium in the sample. However, it would be unlikely that any lithium containing secondary phases would be seen in the X-ray diffraction patterns, as they would be beyond the detection limit of the technique. In order, to deduce which mechanism operates in the present case it is helpful to examine the predicted change in unit cell volume for the three mechanisms. The ionic radii for the species involved are 0.640, 0.79, 0.605 and 0.670 Å for V^{3+}, V^{2+}, Ti^{4+} and Ti^{3+}, respectively, for the ions in six-fold coordination with oxide ions [27]. This means that mechanisms 2 and 3 would be expected to result in larger unit cell volumes, while mechanism 1 would be expected to yield a smaller unit cell volume. Therefore the results of the present study are consistent with mechanisms 2 and 3.

Further evidence for the charge compensation mechanism can be found in the thermogravimetric data. Fig. 2 shows the DTA/TGA thermograms for the studied compositions. The initial weight loss of around 1 to 2% at *ca*. 100°C can be attributed to a small amount of adsorbed water in the powder samples. At temperatures above *ca*. 300°C, both samples show significant weight losses (6.24% for LVT10PC and 4.54% for LVT15PC) associated with the exothermic burning of the carbon coating. In both cases the TGA traces reach a minimum at around 520°C followed by an exothermic mass gain, associated with oxidation. Primarily, this oxidation is of V^{III}, however the

small feature seen in the trace for the $x = 0.1$ composition at around 580°C appears more significant in the $x = 0.15$ composition and suggests that this process has at least two stages, which is again consistent with mechanisms 2 and 3. The existence of VO as a small secondary component in the samples suggests that the conditions used in the experiment readily stabilise divalent vanadium.

TEM images of the studied samples are shown in Fig. 3. Besides the thin layer of carbon coating, the two materials show amounts of carbon (red arrows) around the active material particles. The particle (cluster) size varies significantly from 0.2-8 µm for LVT10PC and 0.5-10 µm for LVT15PC (darker particles in Figs. 3a and 3c). The average particle size distribution is in the range 0.5-1.5 µm and 2-10 µm for LVT10PC and LVT15PC respectively. This is supported by specific surface area measurements, which show values of 55.64 $m^2\ g^{-1}$ and 42.48 $m^2\ g^{-1}$ for the $x = 0.1$ and 0.15 compositions, respectively.

Cyclic voltammagrams for the studied composites are presented in Fig. 4. Both voltammagrams show oxidation potentials at around 3.62, 3.70, 4.12, with the fourth oxidation peak at 4.57 and 4.55 V for LVT10PC and LVT15PC, respectively. The four peaks are associated with the four stages of Li de-intercalation and the corresponding oxidation of vanadium [14]. The third and fourth peaks in the oxidation curve are replaced by a single broad peak at around 3.9 V on reduction. In the titanium substituted samples, this reduction peak occurs at lower potential than in the unsubstituted parent compound [14], which is observed at 4.03 V. The last two reduction peaks are at around 3.63 and 3.56 V. The hysteresis in observed in oxidation and reduction has been examined in detail in the parent LVP material by Yin et al. [24]. Using ^{7}Li solid state NMR and neutron diffraction, these authors showed that vanadium charge distribution and Li site ordering is lost on full de-intercalation (charge) and that on subsequent intercalation (discharge), the Li^+ ions statistically distribute themselves over two sites until vanadium charge and lithium ordering are restored at a composition around $Li_{1.25}V_2(PO_4)_3$.

Second cycle charge-discharge curves for the test cells at 0.2C rate in the range of 2.8–4.4 V are shown in Fig. 5. The samples show three charge-discharge plateaus, in this voltage range, corresponding to the intercalation/de-intercalation of two lithium ions per formula unit [14]. LVT10PC shows a specific discharge capacity of 120.6 mA h g^{-1} in the second cycle, achieving 91.6% of its theoretical capacity for two intercalated lithium ions (131.6 mA h g^{-1}). In our previous study of the carbon coated unsubsituted material under identical conditions to those in the present work, a second cycle discharge capacity of 116.5 mA h g^{-1} was observed [28]. The most heavily substituted composition, LVT15PC shows a lower discharge capacity of 106.2 mA h g^{-1} (2^{nd} cycle). The polarizations of the charge-discharge plateaus vary in the range 50-60 mV for LVT10PC and LVT15PC.

The cycling performance of the studied compositions is summarised in Fig. 6. LVT10PC shows a discharge capacity of 121 mA h g^{-1} in the first cycle, which declines to 115.7 mA h g^{-1}, up to the 60^{th} cycle, corresponding to a 4.4% loss. Compared to our previous studies of the unsubstituted system LVPC [28], LVT10PC shows an improvement in cycling performance (initial discharge capacity 118 mA h g^{-1} and a 6.2% loss over the first 60 cycles in LVPC). LVT15PC displays the lowest initial capacity of 106.7 mA h g^{-1} of the test samples. The differences in initial capacity may be associated with differences in the average particle sizes seen in the TEM. The cycling performance of LVT15PC shows a capacity fade of 7.9% up to 60 cycles. The coulombic efficiencies vary in the range 94-98% and 93-98% for LVT10PC and LVT15PC, respectively.

4. Conclusions

Titanium can successfully be substituted for vanadium in $Li_3V_2(PO_3)_3$. The solid solution mechanism appears to involve reduction of V or Ti rather than formation of lithium vacancies, leaving the theoretical discharge capacity high. Compared to the carbon coated unsubstituted system, LVP, low levels of substitution show improved electrochemical performance, with higher initial discharge capacity and lower capacity fading. Further substitution has a negative impact on initial discharge capacity and capacity loss. This effect may be partly attributable to the larger average particle size and in more heavily substituted compositions. The smaller particle size provides a shorter distance for the lithium ion to diffuse into the particle core [2].

Acknowledgements

This study was supported by Project BG051PO001/3.3-05-0001 “Science and Business”, “Human Resources Development” Operational Programme co-financed by the European Social Fund of the EU and the Bulgarian national budget.

We wish to thank Dr R.M. Wilson at Queen Mary University of London for his help in X-ray data collection.

References

1. Mizushima K, Jones PC, Wiseman PJ, Goodenough JB (1980) Li_xCoO_2 ($0 < x \leq 1$): A new cathode material for batteries of high energy density. Materials Research Bulletin 15 (6):783-789. doi:http://dx.doi.org/10.1016/0025-5408(80)90012-4
2. Padhi AK, Nanjundaswamy KS, Goodenough JB (1997) Phospho-olivines as Positive-Electrode Materials for Rechargeable Lithium Batteries. Journal of The Electrochemical Society 144 (4):1188-1194. doi:10.1149/1.1837571
3. Barker J, Saidi Y (1999) Lithium-containing phosphates, method of preparation, and use thereof. US Patent 5,871,866
4. Rui X, Yan Q, Skyllas-Kazacos M, Lim TM (2014) $Li_3V_2(PO_4)_3$ cathode materials for lithium-ion batteries: A review. Journal of Power Sources 258:19-38. doi:10.1016/j.jpowsour.2014.01.126
5. Bakenov Z, Taniguchi I (2010) Electrochemical performance of nanocomposite $LiMnPO_4$/C cathode materials for lithium batteries. Electrochemistry Communications 12 (1):75-78. doi:http://dx.doi.org/10.1016/j.elecom.2009.10.039
6. Amine K, Yasuda H, Yamachi M (2000) Olivine $LiCoPO_4$ as 4.8 V Electrode Material for Lithium Batteries. Electrochemical and Solid-State Letters 3 (4):178-179. doi:10.1149/1.1390994
7. Wolfenstine J, Allen J (2005) Ni^{3+}/Ni_{2+} redox potential in $LiNiPO_4$. Journal of Power Sources 142 (1–2):389-390. doi:http://dx.doi.org/10.1016/j.jpowsour.2004.11.024
8. Barker J, Gover RKB, Burns P, Bryan A, Saidi MY, Swoyer JL (2005) Structural and electrochemical properties of lithium vanadium fluorophosphate, $LiVPO_4F$. Journal of Power Sources 146 (1–2):516-520. doi:http://dx.doi.org/10.1016/j.jpowsour.2005.03.126
9. Morgan D, Van der Ven A, Ceder G (2004) Li Conductivity in Li_xMPO_4 (M = Mn, Fe, Co, Ni) Olivine Materials. Electrochemical and Solid-State Letters 7 (2):A30-A32. doi:10.1149/1.1633511
10. Rissouli K, Benkhouja K, Ramos-Barrado JR, Julien C (2003) Electrical conductivity in lithium orthophosphates. Materials Science and Engineering: B 98 (3):185-189. doi:http://dx.doi.org/10.1016/S0921-5107(02)00574-3
11. Wang L, Tang Z, Ma L, Zhang X (2011) High-rate cathode based on Li3V2(PO4)3/C composite material prepared via a glycine-assisted sol–gel method. Electrochemistry Communications 13 (11):1233-1235. doi:http://dx.doi.org/10.1016/j.elecom.2011.08.036
12. Li Y, Hong L, Sun J, Wu F, Chen S (2012) Electrochemical performance of Li3V2(PO4)3/C prepared with a novel carbon source, EDTA. Electrochimica Acta 85:110-115. doi:http://dx.doi.org/10.1016/j.electacta.2012.08.038
13. Lan Y, Wang X, Zhang J, Zhang J, Wu Z, Zhang Z (2011) Preparation and characterization of carbon-coated LiFePO4 cathode materials for lithium-ion batteries with resorcinol–formaldehyde polymer as carbon precursor. Powder Technology 212 (2):327-331. doi:http://dx.doi.org/10.1016/j.powtec.2011.06.005
14. Saïdi MY, Barker J, Huang H, Swoyer JL, Adamson G (2003) Performance characteristics of lithium vanadium phosphate as a cathode material for lithium-ion batteries. Journal of Power Sources 119–121:266-272. doi:http://dx.doi.org/10.1016/S0378-7753(03)00245-3
15. Tang A, Wang X, Liu Z (2008) Electrochemical behavior of Li3V2(PO4)3/C composite cathode material for lithium-ion batteries. Materials Letters 62 (10–11):1646-1648. doi:http://dx.doi.org/10.1016/j.matlet.2007.09.064
16. Li Y-Z, Zhou Z, Ren M-M, Gao X-P, Yan J (2007) Improved electrochemical Li insertion performances of Li3V2(PO4)3/carbon composite materials prepared by a sol–gel route. Materials Letters 61 (23–24):4562-4564. doi:http://dx.doi.org/10.1016/j.matlet.2007.02.057
17. Chen Y, Zhao Y, An X, Liu J, Dong Y, Chen L (2009) Preparation and electrochemical performance studies on Cr-doped $Li_3V_2(PO_4)_3$ as cathode materials for lithium-ion batteries. Electrochimica Acta 54 (24):5844-5850. doi:http://dx.doi.org/10.1016/j.electacta.2009.05.041
18. Yuan W, Yan J, Tang Z, Sha O, Wang J, Mao W, Ma L (2012) Mo-doped Li3V2(PO4)3/C cathode material with high rate capability and long term cyclic stability. Electrochimica Acta 72:138-142. doi:http://dx.doi.org/10.1016/j.electacta.2012.04.030
19. Zhong S, Liu L, Jiang J, Li Y, Wang J, Liu J, Li Y (2009) Preparation and electrochemical properties of Y-doped Li3V2(PO4)3 cathode materials for lithium batteries. Journal of Rare Earths 27 (1):134-137. doi:http://dx.doi.org/10.1016/S1002-0721(08)60207-0
20. Son JN, Kim SH, Kim MC, Kim GJ, Aravindan V, Lee YG, Lee YS (2013) Superior charge-transfer kinetics of NASICON-type Li3V2(PO4)3 cathodes by multivalent Al3+ and Cl− substitutions. Electrochimica Acta 97:210-215. doi:http://dx.doi.org/10.1016/j.electacta.2013.02.118
21. Mateyshina YG, Uvarov NF (2011) Electrochemical behavior of Li3−xM`xV2−yM``y(PO4)3 (M`=K, M`` = Sc, Mg+ Ti)/C composite cathode material for lithium-ion batteries. Journal of Power Sources 196 (3):1494-1497.

doi:http://dx.doi.org/10.1016/j.jpowsour.2010.08.078
22. Liu S-Q, Li S-C, Huang K-L, Chen Z-H (2007) Effect of Doping Ti^{4+} on the Structure and Performances of $Li_3V_2(PO_4)_3$. Acta Physico-Chimica Sinica 23 (4):537-542
23. Larson AC, Von Dreele RB (1987) General Structure Analysis System (GSAS). Los Alamos National Laboratory,
24. Yin SC, Grondey H, Strobel P, Anne M, Nazar LF (2003) Electrochemical Property: Structure Relationships in Monoclinic $Li_{3-y}V_2(PO_4)_3$. Journal of the American Chemical Society 125 (34):10402-10411. doi:10.1021/ja034565h
25. Loehman RE, Rao CNR, Honig JM (1969) Crystallography and defect chemistry of solid solutions of vanadium and titanium oxides. The Journal of Physical Chemistry 73 (6):1781-1784. doi:10.1021/j100726a025
26. Huang C, Chen D, Huang Y, Guo Y (2013) Sol–gel synthesis of $Li_3V_2(PO_4)_3$ cathode materials with high electrical conductivity. Electrochimica Acta 100:1-9. doi:http://dx.doi.org/10.1016/j.electacta.2013.03.073
27. Shannon R (1976) Revised effective ionic radii and systematic studies of interatomic distances in halides and chalcogenides. Acta Crystallographica Section A 32 (5):751-767. doi:10.1107/S0567739476001551
28. Stankov SM, Momchilov A, Abrahams I, Popov I, Stankulov T, Trifonova A (2014) Synthesis and Characterisation of Si and Mg Substituted Lithium Vanadium(III) Phosphate. Bulgarian Chemical Communications, in press.

Figure and Table Captions

Fig. 1. Fitted diffraction profiles for (a) LVT10PC and (b) LVT15PC showing observed (+ symbols), calculated (line) and difference (lower) profiles. Reflection positions are indicated by markers (lower = primary phase, upper = secondary phase)

Table 1. Crystal and refinement parameters for $Li_3V_{1.9}Ti_{0.1}(PO_4)_3$-C and $Li_3V_{1.85}Ti_{0.15}(PO_4)_3$-C. Estimated standard deviations are given in parentheses

Fig. 2. Combined TG/DTA thermograms for (a) LVT10PC and (b) LVT15PC

Fig. 3. TEM micrographs of (a, b) LVT10PC and (c, d) LVT15PC. Arrows indicate carbon.

Fig. 4. Cyclic voltammagrams for LVT10PC and LVT15PC in the voltage range 2.8-4.4 V vs. Li/Li^+ with step rate 20 $\mu V\ s^{-1}$

Fig. 5 Second cycle charge-discharge profiles for LVT10PC and LVT15PC at 0.2C rate in the voltage range 2.8-4.4 V vs. Li/Li^+

Fig. 6. Discharge capacities of LVT10PC and LVT15PC recorded during cycling at 0.2C rate in voltage range 2.8–4.4 V vs. Li/Li^+

Figures and Tables

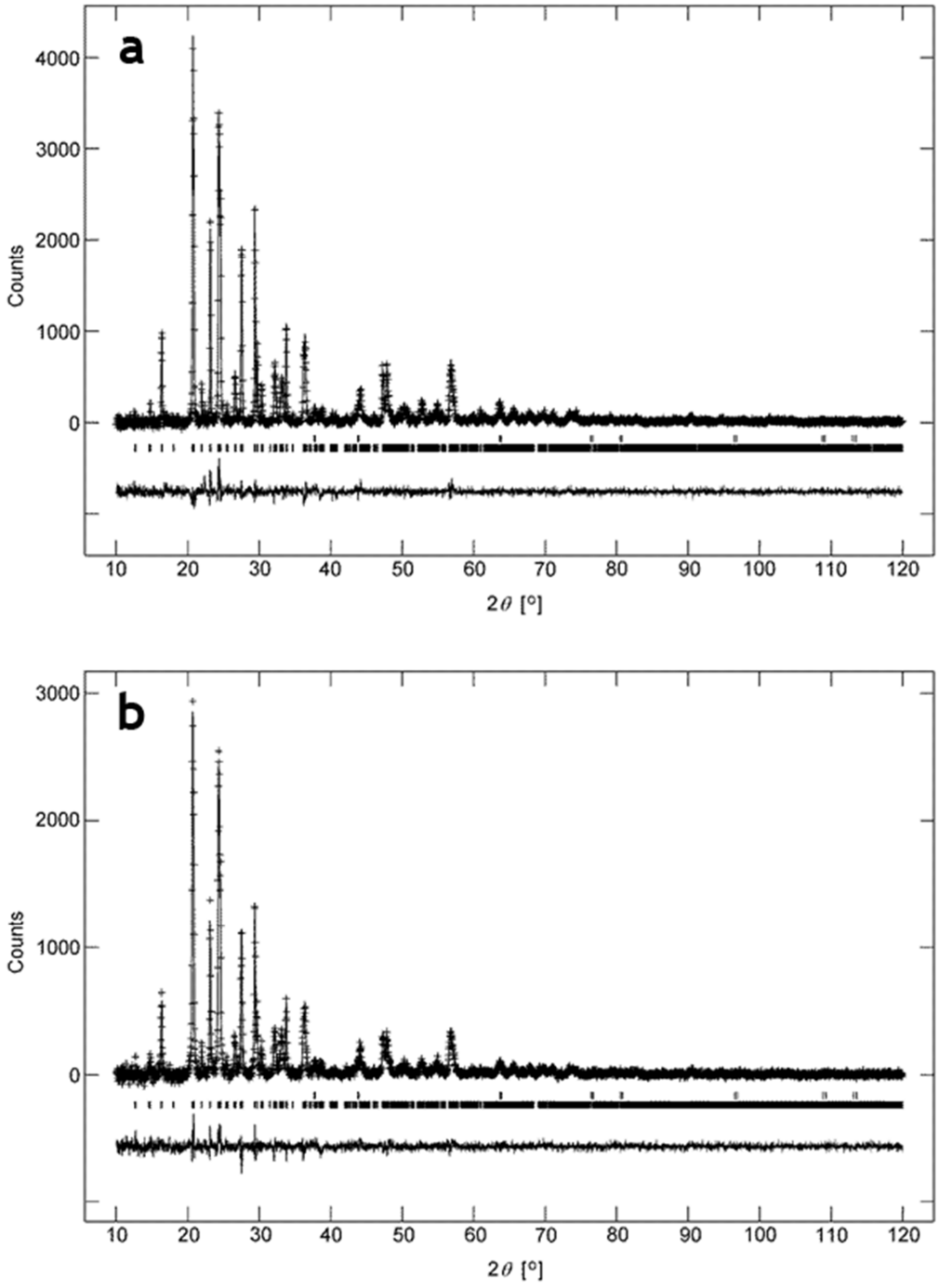

Fig. 1.

Table 1

Acronym	LVT10PC	LVT15PC
Sample description	Black powder	Black powder
R-factors[a]	R_{wp} = 0.0771, R_p = 0.0573 R_{ex} = 0.0597, R_F2 = 0.1161 χ^2 = 1.696	R_{wp} = 0.0706, R_p = 0.0522 R_{ex} = 0.0608, R_F2 = 0.1700 χ^2 = 1.37
No. of variables	51	51
No of profile points used	3290	3290
No of reflections	2707	2725
(a) Primary Phase		
Empirical formula	$Li_3O_{12}P_3Ti_{0.1}V_{1.9}$	$Li_3O_{12}P_3Ti_{0.15}V_{1.85}$
Formula weight	407.31 g mol^{-1}	407.16 g mol^{-1}
Crystal system	Monoclinic	Monoclinic
Space group	$P2_1/n$	$P2_1/n$
Unit cell dimension	a = 8.5907(4) Å b = 8.6030(3) Å c = 12.0266(4) Å β = 90.390(3)°	a = 8.5937(7) Å b = 8.5985(6) Å c = 12.0328(9) Å β = 90.450(5)°
Volume	888.82(7) Å^3	889.1(2) Å^3
Z	4	4
Density (calculated)	3.042 Mg m^{-3}	3.038 Mg m^{-3}
Weight fraction	0.98803(7)	0.98949(8)
(b) Secondary phase		
Empirical formula	VO	VO
Formula weight	66.94 g mol^{-1}	66.94 g mol^{-1}
Crystal system	Cubic	Cubic
Space group	Fm-3m	Fm-3m
Unit cell dimension	a = 4.1306(3) Å	a = 4.1272(6) Å
Volume	70.48(2) Å^3	70.30(3) Å^3
Z	4	4
Density (calculated)	6.309 Mg m^{-3}	6.324 Mg m^{-3}
Weight fraction	0.0120(6)	0.0105(7)

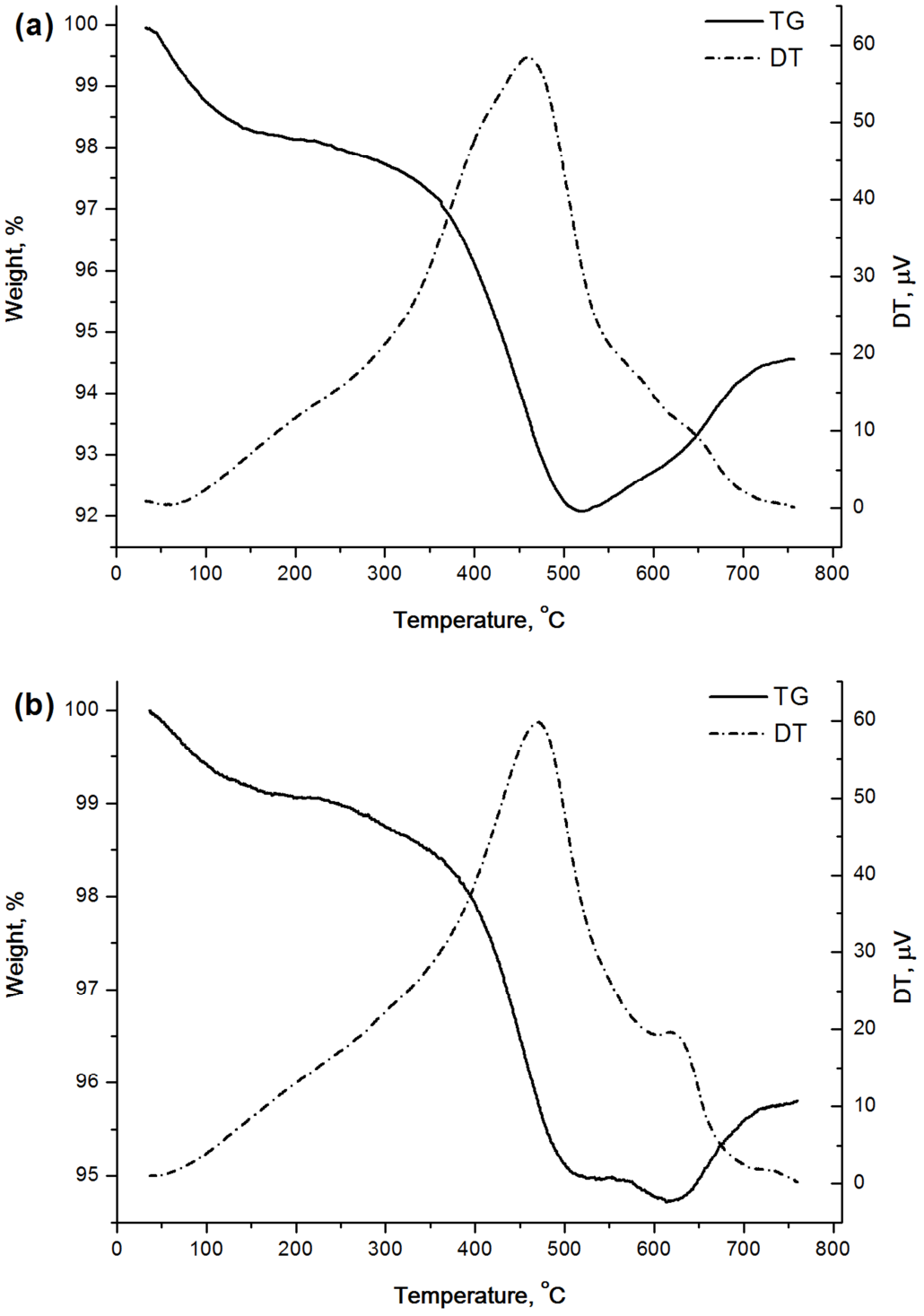
(a)
TG
DT
Weight, %
DT, μV
Temperature, °C
(b)
TG
DT
Weight, %
DT, μV
Temperature, °C

Fig. 2.

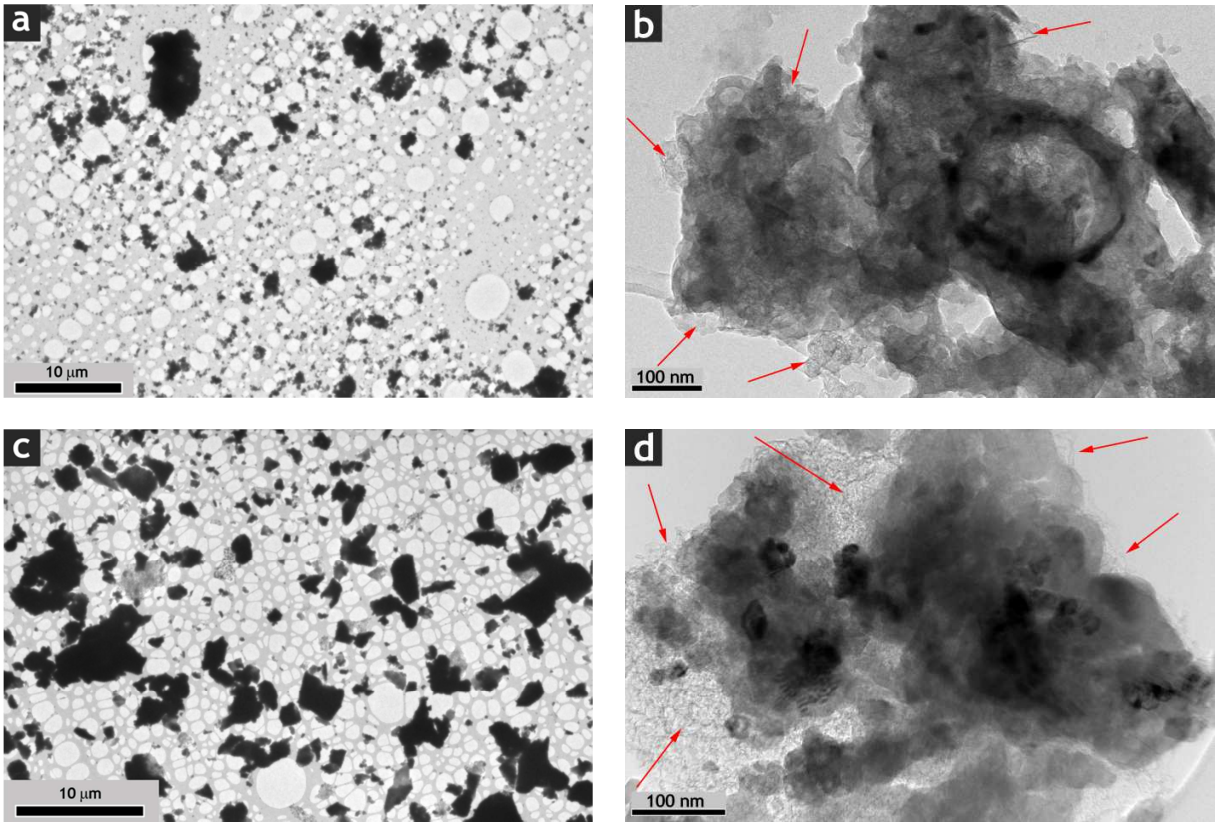

Fig. 3.

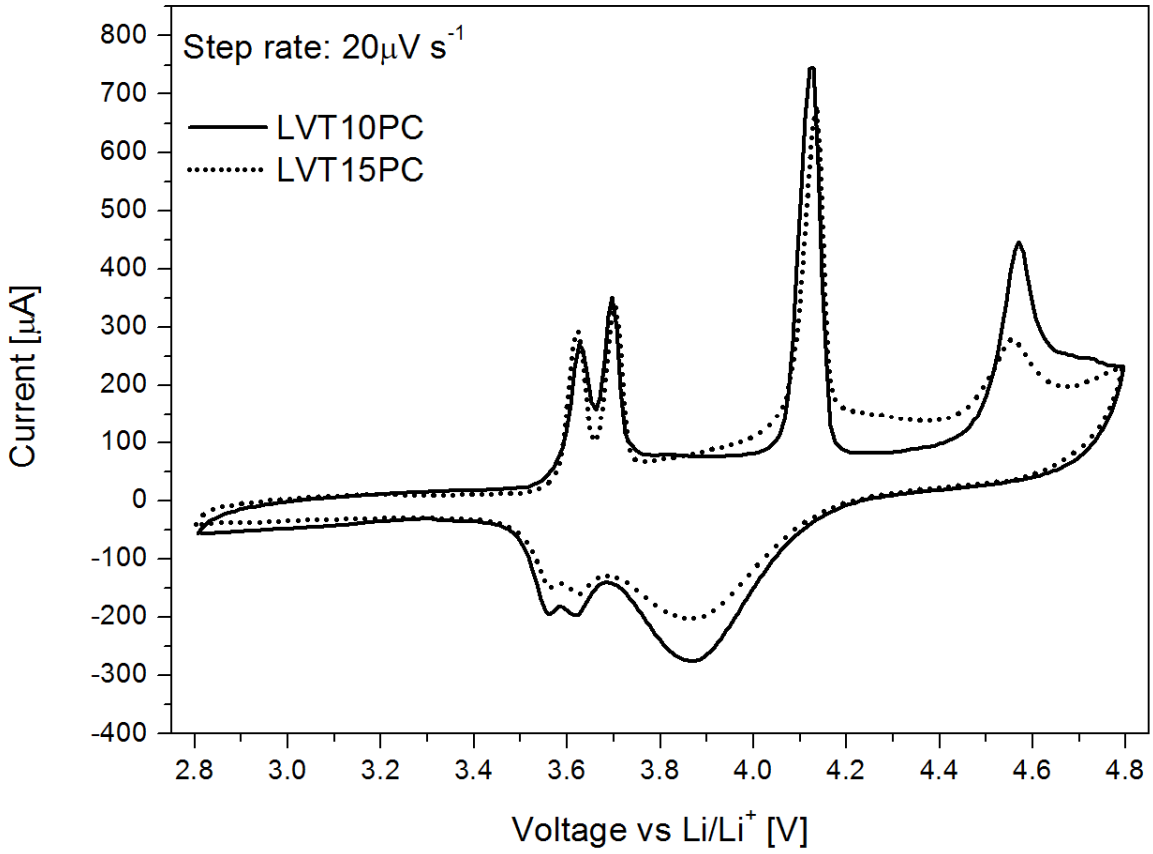
Step rate: 20μV s-1
LVT10PC
LVT15PC
Current [μA]
Voltage vs Li/Li+ [V]
800
700
600
500
400
300
200
100
0
-100
-200
-300
-400
2.8
3.0
3.2
3.4
3.6
3.8
4.0
4.2
4.4
4.6
4.8

Fig. 4.

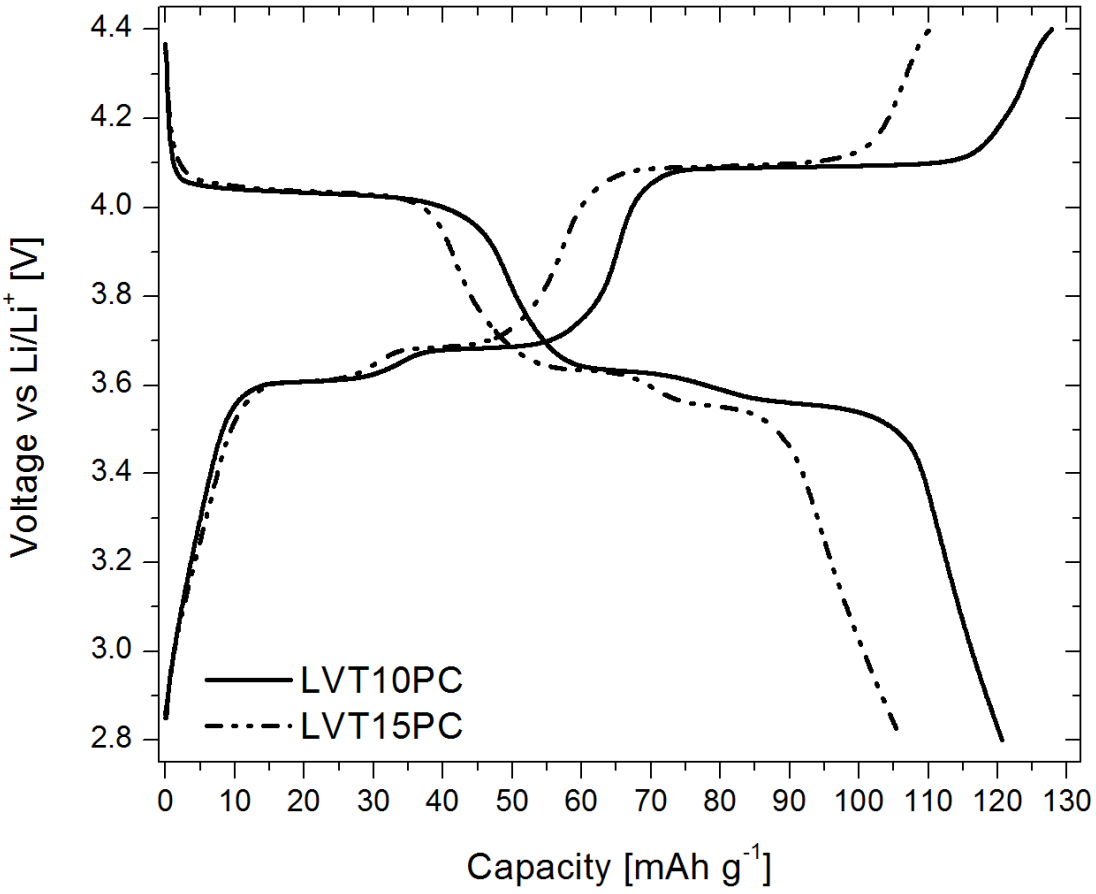
Voltage vs Li/Li+ [V]
Capacity [mAh g-1]
LVT10PC
LVT15PC
4.4
4.2
4.0
3.8
3.6
3.4
3.2
3.0
2.8
0
10
20
30
40
50
60
70
80
90
100
110
120
130

Fig. 5.

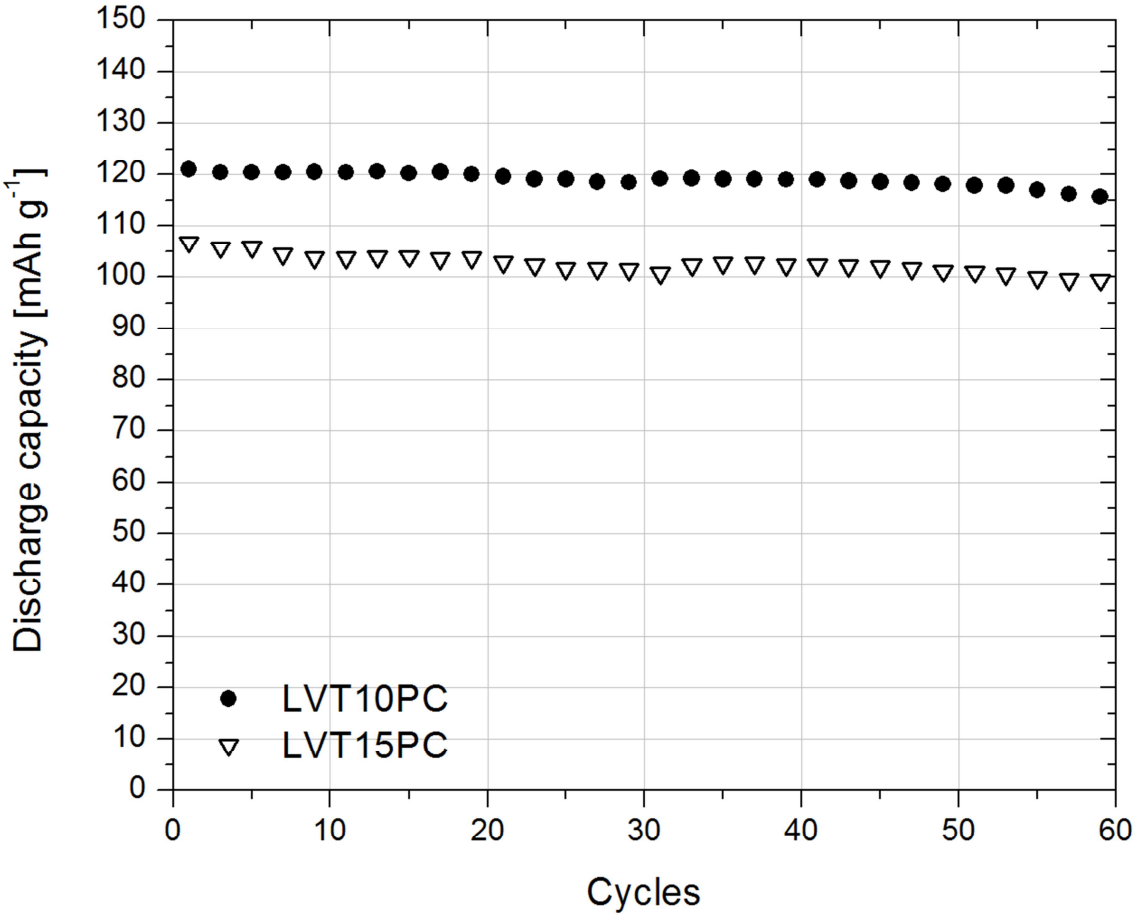
Discharge capacity [mAh g-1]
Cycles
LVT10PC
LVT15PC
0
10
20
30
40
50
60
70
80
90
100
110
120
130
140
150

Fig. 6.